Available online at www.sciencedirect.com
SCIENCE DIRECT
ELSEVIER
Ultramicroscopy 106 (2006) 881–887
ultramicroscopy
www.elsevier.com/locate/ultramic

# Components for high speed atomic force microscopy

Georg E. Fantner[a,*], Georg Schitter[a,1], Johannes H. Kindt[a,1], Tzvetan Ivanov[b,1], Katarina Ivanova[b], Rohan Patel[a], Niels Holten-Andersen[c], Jonathan Adams[a], Philipp J. Thurner[a], Ivo W. Rangelow[b], Paul K. Hansma[a]

[a]*Department of Physics, University of California Santa Barbara, CA 93106, USA*
[b]*Institute for Microstructuring, University Kassel, D-34132, Germany*
[c]*Biomolecular Science and Engineering, University of California Santa Barbara, CA 93106, USA*

Received 17 September 2005; accepted 23 January 2006

**Abstract**

Many applications in materials science, life science and process control would benefit from atomic force microscopes (AFM) with higher scan speeds. To achieve this, the performance of many of the AFM components has to be increased. In this work, we focus on the cantilever sensor, the scanning unit and the data acquisition. We manufactured 10 μm wide cantilevers which combine high resonance frequencies with low spring constants (160–360 kHz with spring constants of 1–5 pN/nm). For the scanning unit, we developed a new scanner principle, based on stack piezos, which allows the construction of a scanner with 15 μm scan range while retaining high resonance frequencies (>10 kHz). To drive the AFM at high scan speeds and record the height and error signal, we implemented a fast Data Acquisition (DAQ) system based on a commercial DAQ card and a LabView user interface capable of recording 30 frames per second at 150 × 150 pixels.


*PACS:* 07.79.Lh; 62.25.+g; 87.64.Dz; 85.85.+j

*Keywords:* Atomic force microscopy (AFM); Tip scanning instrument design and characterization; Instrument control and alignment

## 1. Introduction

The possibilities for high speed atomic force microscopy (AFM) have been impressively demonstrated by several groups since the 1990s [1–8]. Great technological advances have been made in the areas of sensitive low noise cantilever sensors [9,10], faster cantilevers [11], high rigidity scanners [12,13] and control schemes [14–16]. The applications in which high speed AFM has been successfully used, however, are limited, since only a small number of dedicated research labs have high speed AFM capability, and these instruments are highly specialized. The need arises for a versatile, easy to use AFM that allows higher imaging speeds for a broader range of applications. In this work, we discuss three areas necessary for high speed AFM and present modular solutions that allow for the increase of AFM imaging speeds.

## 2. Small cantilevers

Higher speed AFM puts greater demands on the detection of the interaction between the sample and the cantilever sensor. As with all sensors, the speed performance of the sensor is limited by the sensor bandwidth. For a cantilever sensor, the maximum scan speed is determined by the spring constant, the effective mass of the cantilever, the damping of the cantilever in the surrounding medium, and the sample stiffness. The maximum achievable scan rates are

$$v \ll \frac{\lambda D}{2m} \tag{1}$$

*Corresponding author.
*E-mail address:* fantner@physics.ucsb.edu (G.E. Fantner).
[1]These authors have contributed equally to this work.

0304-3991/$ - see front matter © 2006 Published by Elsevier B.V.
doi:10.1016/j.ultramic.2006.01.015

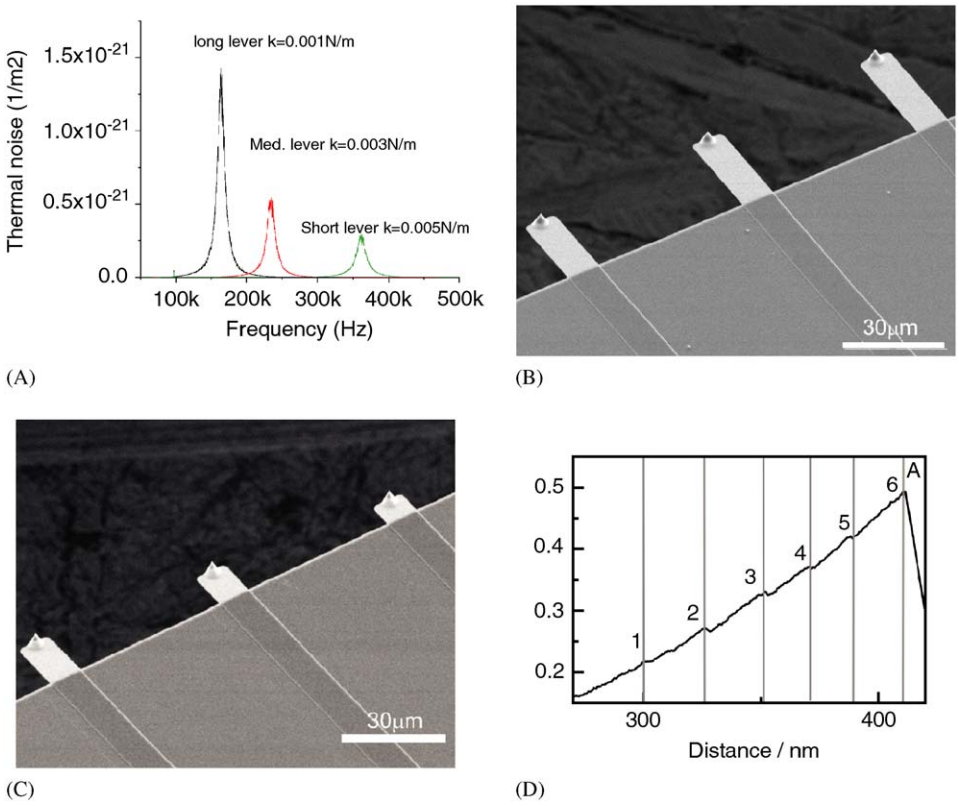


Fig. 1. Smaller cantilevers give higher speed performance and allow lower noise measurements. (A) Thermal spectra of small cantilevers. (B) Batch fabricated 10 μm wide cantilevers with integrated tips. These cantilevers have a length of 25, 30 and 35 μm, respectively, and are designed for contact mode imaging. (C) Small cantilevers for tapping mode imaging. These cantilevers have a length of 10, 15 and 20 μm, respectively. (D) Molecular force spectroscopy curve taken on a collagen fibril with 5 μm wide levers reveal a fine structure in the pulling curve that was not observable with conventional cantilevers [19].

or

$$v \ll \frac{\lambda}{2}\sqrt{\frac{k+S}{m}-\frac{D^2}{2m^2}}, \tag{2}$$

where $v$ is the maximum achievable velocity, $\lambda$ the periodicity of surface features, $D$ the damping, $k$ the spring constant, $m$ the effective cantilever mass, $S$ the surface elasticity, for the cases of low damping and high damping, respectively [17]. From Eqs. (1) and (2) it is clear that the maximum achievable scan speed increases if the mass of the cantilever is reduced by making the cantilever smaller. A cantilever with the dimensions $25\,\mu m \times 10\,\mu m \times 0.1\,\mu m$ having a mass of 77 pg can (according to Eq. (1)) image a sample 10 times faster, compared to the smallest cantilevers currently commercially available (to our knowledge the Olympus biolevers). It also has been shown that making the cantilever smaller reduces the noise for a given bandwidth in the cantilever measurement [18]. For these reasons we have manufactured cantilevers 10 μm wide, 100 nm thick and with various lengths (see Fig. 1(A) and (B)). These cantilevers have resonance frequencies ($f_0$) in air between 150 and 350 kHz with spring constants between 0.001 and 0.005 N/m. The Q-factors in air are between 13 and 21. The cantilevers are fabricated from a low stress SiN composite. These small cantilevers have batch produced integrated tips, unlike the cantilevers we previously made in our lab [9] where the tips were individually deposited by electron beam deposition (EBD) [10]. Fig. 1(C) shows cantilevers intended for tapping mode. These cantilevers have resonance frequencies of up to 2 MHz while still keeping spring constants below 2 N/m. Fig. 1(D) from Ref. [19] shows a pulling curve taken with a 5 μm wide cantilever on whole collagen fibrils from a rat tail tendon.The reduced noise of the small cantilever allowed to observe small force ruptures within the pulling spectrum.

Fig. 2 shows tapping mode images of plasmid DNA acquired with a 10 μm wide cantilever ($f_0 = 263$ kHz) using a prototype small cantilever head[2] and scanning at 8 Hz line rate. The width of the DNA molecules gives an upper bound for the tip sharpness of the small cantilevers to be 6 nm. For higher line-scan rates in tapping mode imaging, cantilevers with an even higher ratio of $Q/f_0$ [20] will be required.

## 3. High rigidity scanner design

One of the factors that limit the scan speed in commercial AFMs is the low mechanical resonance frequency of most commercial systems. The triangular

[2]Courtesy of Veeco Metrology Inc., Santa Barbara, CA.

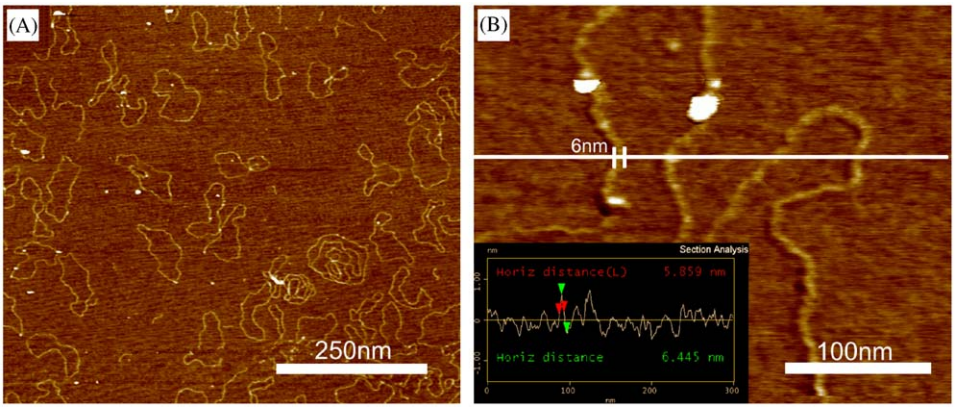


Fig. 2. AFM images of plasmid DNA imaged in tapping mode with 10 μm wide cantilevers. (A) Overview image taken at 8 lines per second. (B) A higher magnification image gives an upper bound for the tip sharpness to be 6 nm.

shaped scan signal that is used in most systems contains many higher order Fourier components which can excite the resonances of the scanner. This results in image distortion in the $X$ and $Y$ directions as well as the $Z$ direction and limits the scan speed to $\approx 1\%$ of the lateral resonance frequency of the scanner, unless these resonances are actively compensated [16]. In order to avoid these complications, two elegant approaches have been demonstrated:

*Scan at the resonance frequency of the scanner*: this approach has been successfully used to record high speed SNOM and AFM images [21,8]. While this approach allows large scan sizes, it does not allow to change the scan speed easily during the experiment. Also, due to the nature of this approach, the scan motion is sinusoidal rather than the predominately used triangular scan motion. This results in the need to deconvolute the data. Different scan speeds at the center of the image compared to the edges of the image result in a nonconstant force interaction between the tip and the sample. Also, in this approach, it is not possible to rotate the scan direction.

*Increase the resonance frequencies*: in this approach, scanners are designed so that their mechanical resonance frequencies are much higher than those of conventional scanners [6,13]. These high resonance frequency scanners have the advantages of conventional AFM scanners with regards to changes in scan speed. They also allow triangular scanning motion. However, up until now, this approach often limited the scan size of these AFM scanners, which reduces their usability to a limited set of applications.

In our work, we tried to develop an AFM scanner that is suitable for most biological AFM applications and has high-speed imaging capabilities. To meet these requirements this scanner has to have high first mechanical resonance frequencies ($>10$ kHz), while maintaining a scan-range of about 15 μm in $X$- and $Y$-directions, and full control over the scanning motion to allow for linear scans and scan rotation.

Fig. 3 illustrates the basic principle of our design. We use 1D multilayer piezo stacks (Tokin-NEC, Sendai City, Japan) as actuators which are coupled together to form a 3D scanner by comb-flexures. The comb-flexure (Fig. 3(A)) consists of an array of vertical blade springs that are stiff in the direction of movement of the attached piezo, and flexible in one of the perpendicular directions. We use two piezos per axis, which are actuated by complementary signals. When one of the two piezos expands, the opposite piezo contracts, which results in a net movement of the center of the scanner (see Fig. 3(A)). The outer ends of the piezo stacks are attached to a rigid outer support frame while the inner side of the piezos is attached to a partially flexible inner support frame. This inner support frame bends in the direction of actuation when the piezo expands. In the two directions perpendicular to the direction of actuation, however, this frame constrains the piezo stack. This prevents the piezos and the center from oscillating up and down like a trampoline, thereby increasing the resonance frequency in the important $Z$-direction. Fig. 3(B) shows an implementation of this principle where the $Z$-actuation is achieved by a pair of piezo stacks in a balanced configuration [6] attached to the center of the scanner. This scanner has a nominal range of 15 μm in the $X$ and $Y$ directions and 6 μm in $Z$ direction. The scanner is equipped with strain gauge sensors that measure the expansion of the piezos. A closed loop controller is used to linearize the scanner and allow accurate offset and zoom in. This scanner is compatible with a standard multimode head (Veeco Metrology Inc., Santa Barbara, CA). A modified Nanoscope 3a controller and a custom made piezo drive amplifier[3] was used to run the AFM.

To test the performance of this scanner, we imaged a calcite crystal in a liquid environment at 122 lines per second. While imaging, we added concentrated HCl to observe the dissolution of the calcite crystal in a highly

[3]Developed with Techproject partner company, Vienna, Austria, www.techproject.at

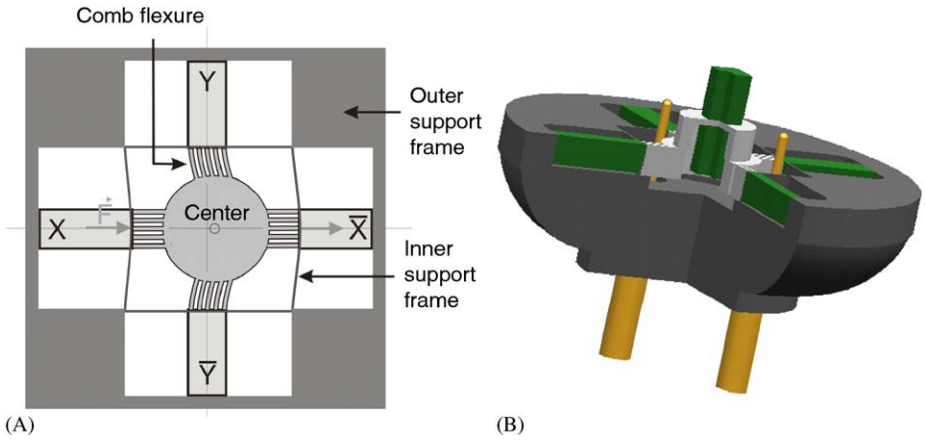


Fig. 3. Design concept based on piezo stacks, which enables larger scan ranges and higher resonance frequencies. (A) The linear actuating piezo stacks are combined to a 3D scanning unit by flexible blade springs (flexures) which are stiff in the axis of actuation and flexible in one of the perpendicular axes. The piezos are attached with one side to a ridged outer support frame and with the other side to a partially flexible inner support frame to suppress resonances in $Z$. (B) Scanner design based on this principle which has a nominal scan size of 15 μm in $X$ and $Y$ and 6 μm in $Z$.

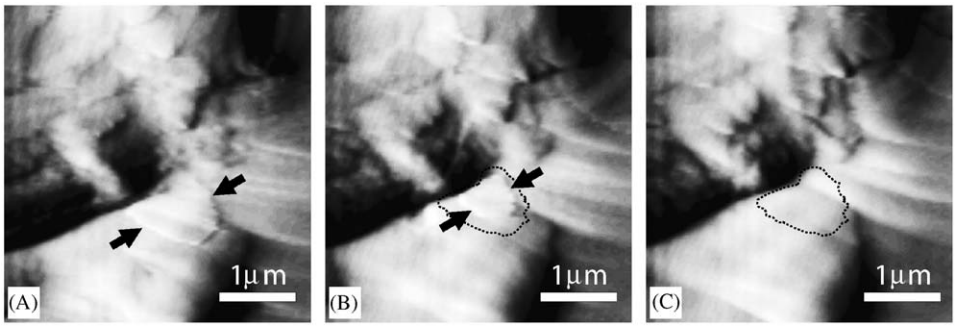


Fig. 4. High speed AFM images (error signal) of the dissolution of a calcite crystal in a nonequilibrium environment after injection of 20% HCl. A stepedge can be seen on the surface (A) which gradually decreases in size (B) until it disappears completely (C). Images are a 4 μm cutout of a 12 μm image.

nonequilibrium environment. Fig. 4 shows the dissolution of the calcite crystal due to the HCl. The initial step edge in the center of the image (Fig. 4(A)) is reduced in size (Fig. 4(B)) and eventually disappears completely. The high scan speed allowed us to observe this dissolution despite the high etch rate. For this experiment, images were taken at approximately 1 frame per second. In Fig. 4 we show every fifth image. Images were taken with conventional Si cantilevers ($k = 40\,\mathrm{N/m}$) in contact mode.

The closed loop operation in $X$, $Y$ and $Z$ of the scanner allows us to accurately and quickly position the cantilever over a specific spot or trajectory of the sample. This allows us to very accurately measure distances on the sample as well as do closed loop AFM indentation and single molecule pulling. Fig. 5 shows AFM indentation experiments on a biocomposite sample extracted from mussel byssus (also called byssal threads). The byssal threads consist of an inner bundle of collagen like fibrils that are the main load bearing component (Fig. 5(A)). The threads are coated with an abrasive resistant coating, which is reinforced with knobby features. Fig. 5(B) shows a magnification of four knobs which were chosen for indentation. The crosses depict the places which were chosen to indent at (using the Nanoscope + PicoForce software feature "point and shoot" in combination with external closed loop feedback). Fig. 5(C) shows the same area imaged after the indentation. The marks the AFM cantilever left are where it was intended. From these experiments on biological samples, as well as spin-coated polymer samples, we estimate the lateral position accuracy of our closed loop system to be ≈ 6 nm at full bandwidth of the $X$, $Y$ feedback.

## 4. Data acquisition

When recording images with a high speed AFM, large amounts of data must be processed in real-time. Three main tasks have to be performed:

- analog to digital conversion of the height and error signals;
- transfer of the data into the computer memory;
- display and/or save the data.

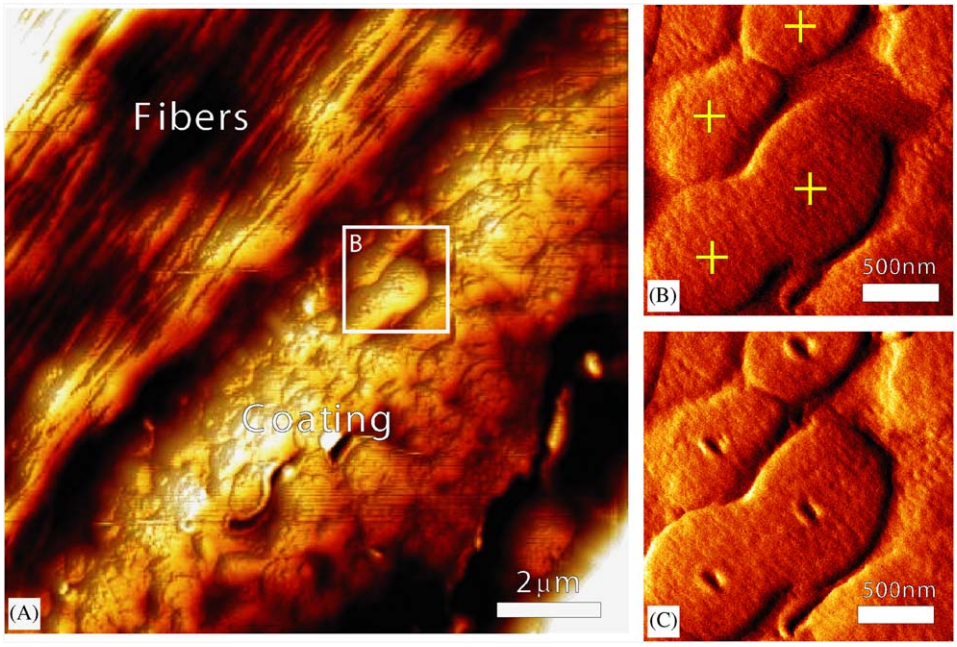


Fig. 5. AFM Indentation on the bio-composite coating of a mussel byssal thread. (A) The tough threads of the mussel byssus are coated by a layer which is reinforced with knobs. (B) Close up of knobs in the coating. The + signs mark the spots where the indentation will be performed. (C) Image of the same area after indentation. The cantilever tip left indents at the previously specified places.

For most current AFM controllers, the large amounts of data that must be transferred and processed significantly limit the scan speeds when using a high speed AFM. In order to circumvent this limitation, we implemented a data acquisition system (DAQ) based on a commercially available DAQ card (Adlink 2002) and LabView 6i (National Instruments, Austin, TX) [22]. The data is streamed over the PCI bus directly into the PC main memory using direct memory access (DMA). By creating the scan signals synchronously with the sampling of the height and deflection data, we minimized the amount of post transfer data processing required to sort the continuous data stream into lines and frames.

Fig. 6 shows the performance of the DAQ system. When sampling the data (A/D conversion), recording and simultaneously displaying the data, we achieved the data rates shown by the red circles. When not simultaneously displaying the data and only saving it to disk, we almost achieved the full 2 MSamples sampling rate of the DAQ card. Due to the requirement of the synchronous D/A and A/D conversion, not all combinations of line rate and pixels per line are possible [22]. We find, however, that the possible combinations are sufficiently close together to use this DAQ system for our high speed AFM experiments. This is shown by comparing the nominal frame rate with the actual frame rate for some common combinations for high speed AFM imaging as listed in Table 1.

To demonstrate the performance we recorded images of two test specimens with this DAQ system and a refined version of the scanner shown in Fig. 3. Fig. 7(A) shows a silicon calibration grating imaged in contact mode at 2060 Hz line rate, i.e., at 4 frames per second (cf. Table 1).

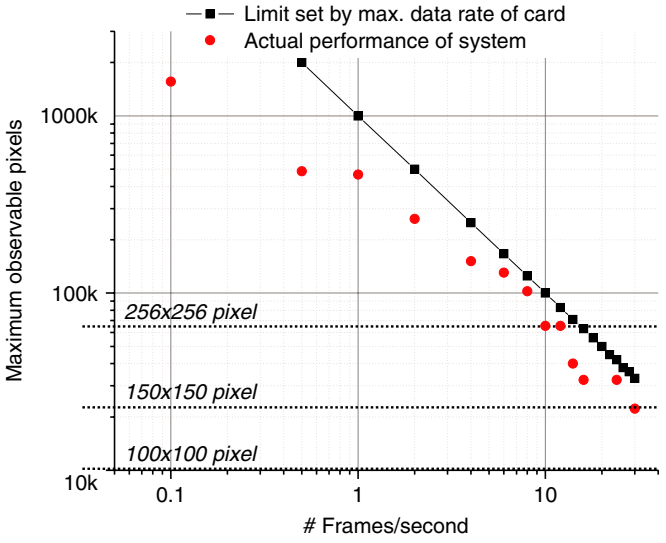


Fig. 6. Performance of our high speed DAQ system. The black squares represent the theoretical maximum based on the 2 MSamples sampling rate of the DAQ card. The red circles represent measured performance levels when processing, displaying and saving the data. [22].

Fig. 7(B) shows images of type I collagen fibrils in air. The scan speed was 1560 lines per second.

## 5. Conclusion

In this work, we have described several improvements we have made for high speed AFM. Using small cantilevers (10 µm wide, 100 nm thick), we increase the bandwidth of the cantilever and reduce its noise power density. A new

Table 1
Some possible combinations of pixel resolution and frame rates of the DAQ system for high speed AFM imaging

| *X*-res. (pixel) | *Y*-res. (pixel) | Nominal frame rate ($s^{-1}$) | Actual frame rate ($s^{-1}$) | Line rate (kHz) | Pixel rate (MHz) |
|---|---|---|---|---|---|
| 256 | 256 | 2 | 2.01 | 1.03 | 0.526 |
| 256 | 256 | 4 | 4.02 | 2.06 | 1.05 |
| 256 | 256 | 8 | 7.63 | 3.91 | 2.00 |
| 128 | 128 | 12 | 12.72 | 3.26 | 0.833 |
| 128 | 128 | 25 | 25.43 | 6.51 | 1.67 |
| 128 | 128 | 30 | 30.5 | 7.81 | 2.00 |

Frame rate indicates down frames only, i.e., twice the rate of frames could be recorded if we record both up and down frames.

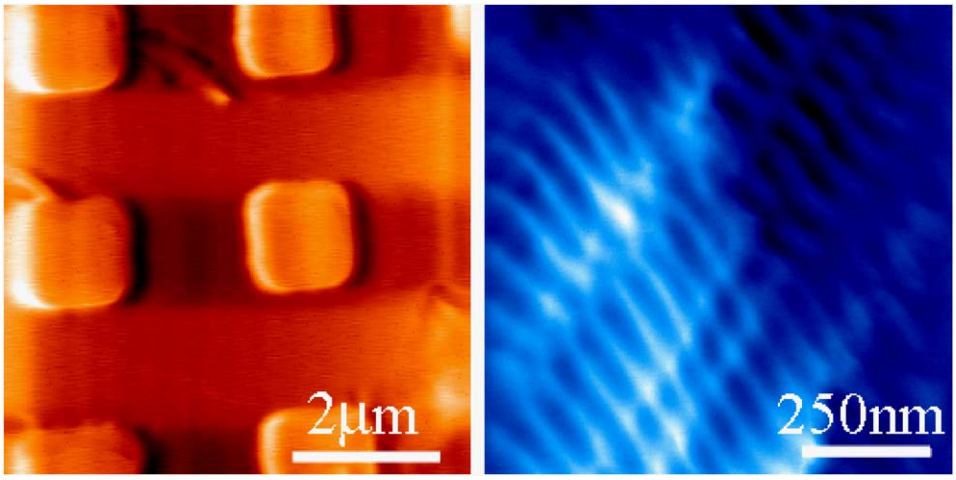


Fig. 7. High speed AFM image of (A) a silicon calibration grating with 44 nm steps and a pitch of 3 μm, recorded at 2060 lines per second and a resolution of 256 × 256 pixels (height data displayed) and (B) type I collagen fibrils at 1560 lines per second which shows the characteristic 67 nm banding periodicity (deflection data displayed).

scanner design concept allows higher scan speeds while still retaining a 15 μm scan size. These two improvements can be used individually, as each will allow an increase of the scan speed compared to conventional systems. A combination of the two, together with the use of a faster DAQ system and improved control methods, will allow for further increases of the scan speed.

## Acknowledgments

This work was supported by the National Science Foundation through the UCSB Materials Research Laboratory under Award DMR00-80034, by the National Institutes of Health under Award GM65354, by the NASA University Research, Engineering and Technology Institute on Bio-inspired Materials under Award no. NCC-1-02037, by a research agreement with Veeco #SB030071, and by the U.S. Army Research Laboratory and the U.S. Army Research Office under contract numbers DAAD19-03-D-0004 and W911QY-04-P-0516. GF thanks the Austrian Academy of Science for a DOC fellowship, GS thanks the FWF for support under Project no. J2395-N02, and PT acknowledges SNF fellowship no. PBEZ2-105116.

## References

[1] R.C. Barett, C.F. Quate, J. Vac. Sci. Technol. B 9 (2) (1991) 302.
[2] P.E. Hillner, A.J. Gratz, S. Manne, P.K. Hansma, Geology 20 (4) (1992) 359.
[3] G.T. Paloczi, B.L. Smith, P.K. Hansma, D.A. Walters, M.A. Wendman, Appl. Phys. Lett. 73 (12) (1998) 1658.
[4] T. Sulchek, R. Hsieh, J.D. Adams, S.C. Minne, C.F. Quate, D.M. Adderton, Rev. Sci. Instrum. 5 (71) (2000) 2097.
[5] M.B. Viani, L.I. Pietrasanta, J.B. Thompson, A. Chand, I.C. Gebeshuber, J.H. Kindt, M. Richter, H.G. Hansma, P.K. Hansma, Nat. Struct. Biol. 7 (8) (2000) 644.
[6] T. Ando, N. Kodera, E. Takai, D. Maruyama, K. Saito, A. Toda, Proc. Natl. Acad. Sci. USA 98 (22) (2001) 12468.
[7] J.K. Hobbs, A.D.L. Humphris, M.J. Miles, Macromolecules 34 (16) (2001) 5508.
[8] A.D.L. Humphris, M.J. Miles, J.K. Hobbs, Appl. Phys. Lett. 86 (3) (2005) 034106.
[9] M.B. Viani, T.E. Schaffer, G.T. Paloczi, L.I. Pietrasanta, B.L. Smith, J.B. Thompson, M. Richter, M. Rief, H.E. Gaub, K.W. Plaxco, A.N. Cleland, H.G. Hansma, P.K. Hansma, Rev. Sci. Instrum. 70 (11) (1999) 4300.
[10] J.H. Kindt, G.E. Fantner, J.B. Thompson, P.K. Hansma, Nanotechnology 15 (9) (2004) 1131.
[11] R. Pedrak, T. Ivanov, K. Ivanova, T. Gotszalk, N. Abedinov, I.W. Rangelow, K. Edinger, E. Tomerov, T. Schenkel, P. Hudek, J. Vac. Sci. Technol. 21 (6) (2003) 3102.

[12] T. Ando, N. Kodera, Y. Naito, T. Kinoshita, K. Furuta, Y.Y. Toyoshima, Chem. Phys. Chem. 4 (11) (2003) 1196.
[13] J.H. Kindt, G.E. Fantner, J.A. Cutroni, P.K. Hansma, Ultramicroscopy 100 (3–4) (2004) 259.
[14] D. Croft, G. Shed, S. Devasia, ASME J. Dyn. Syst. Meas. Control 123 (2001) 35.
[15] G. Schitter, F. Allgower, A. Stemmer, Nanotechnology 15 (1) (2004) 108.
[16] G. Schitter, A. Stemmer, IEEE Trans. Control Syst. Technol. 12 (3) (2004) 449.
[17] H.J. Butt, P. Siedle, T.K. Seifer, K. Fendler, T. Seeger, E. Bamberg, A.L. Weisenhorn, K. Goldie, A. Engel, J. Microsc. (Oxford) 169 (1) (1993) 75.
[18] M.B. Viani, T.E. Schaffer, A. Chand, M. Rief, H.E. Gaub, P.K. Hansma, J. Appl. Phys. 86 (4) (1999) 2258.
[19] T. Gutsmann, G.E. Fantner, J.H. Kindt, M. Venturoni, S. Danielsen, P.K. Hansma, Biophys. J. 86 (5) (2004) 3186.
[20] T. Sulchek, G.G. Yaralioglu, S.C. Minne, C.F. Quate, Rev. Sci. Instrum. 73 (8) (2002) 2928.
[21] A.D.L. Humphris, J.K. Hobbs, M.J. Miles, Appl. Phys. Lett. 83 (1) (2003) 6.
[22] G.E. Fantner, P. Hegarty, J.H. Kindt, G. Schitter, G.A.G. Cidade, P.K. Hansma, Rev. Sci. Instrum. 76 (2) (2005) 026118.